THE ASTROPHYSICAL JOURNAL, 415:181–190, 1993 September 20

GASDYNAMICS OF RELATIVISTICALLY EXPANDING GAMMA-RAY BURST SOURCES: KINEMATICS, ENERGETICS, MAGNETIC FIELDS, AND EFFICIENCY

P. MÉSZÁROS,[1] P. LAGUNA,[1] AND M. J. REES[2]
Received 1992 January 5; accepted 1993 March 26

ABSTRACT

We calculate both analytically and numerically the evolution of highly relativistic fireballs through the stages of free expansion and coasting, and determine the dependence of the thermodynamic and radiation variables in the comoving and laboratory frames. The dynamics and the comoving geometry change at the (lab) expansion factors $r/r_0 > \eta$ and $r/r_0 > \eta^2$, respectively, where $\eta = E_0/M_0 c^2$ is the initial Lorentz factor. In the lab, the gas appears concentrated in a thin shell of width r_0 until $r/r_0 \lesssim \eta^2$, and increases linearly after that. Magnetic fields may have been important in the original impulsive event. We discuss their effect on the fireball dynamics and also consider their effects on the radiation emitted when the fireball runs into an external medium and is decelerated. The inverse synchro-Compton mechanism can then yield high radiative efficiency in the reverse shock (and through turbulent instabilities and mixing also in the forward blast wave), producing a burst of nonthermal radiation mainly in the MeV to GeV range. The energy and duration depend on η, the magnetic field strength, and the external density, and can match the range of properties observed in cosmic gamma-ray bursts.

Subject headings: gamma rays: bursts — hydrodynamics — radiation mechanisms: miscellaneous

1. INTRODUCTION

Gamma-ray burst sources (GRBs) have long been suspected to originate from the sudden release of energy in small regions of space, where the initial energy density and characteristic photon energy is so large that an opaque $e^{\pm}$ fireball forms (e.g., Cavallo & Rees 1978; Paczyński 1986; Goodman 1986; Shemi & Piran 1990). If these events were located at distances comparable to (or larger than) typical galactic scales, the $e^{\pm}$ fireballs would necessarily remain optically thick out to radii of at least $\sim 10^9$ cm (e.g., Zdziarski 1982; Imamura & Epstein 1987), depending on the amount of normal electrons and baryons mixed in with the pairs. If the fireball originated in a region smaller than this, the radiation pressure on the optically thick fireball would cause it to expand; the evolution of this fireball was initially thought to lead, when it became optically thin, to the observed gamma-ray bursts. This model has recently received increased attention because the spatial distribution of GRBs revealed by the BATSE experiment on the *Compton Observatory* strongly suggested an extended galactic halo or a cosmological origin (Meegan et al. 1992; Fishman 1992; Hartmann 1992; Paczyński 1992).

In its simplest version, the fireball model failed to account for the duration and time structure of the observed bursts: it predicts a very short burst, emitted when the expanding fireball becomes optically thin (Goodman 1986), and a quasi-thermal, soft γ-ray spectrum (Goodman 1986; Paczyński 1986). Another problem, emphasized by Paczyński 1990, was the possibility that the γ-rays could easily be degraded to even lower energies by adiabatic cooling due to scattering on electrons associated with baryons polluting the pair flow. In fact, in the latter case, most of the fireball energy gets converted into bulk kinetic energy of the polluting baryons, while the photon burst at thinning has much less energy than the initially available one. These problems are removed when one considers anisotropic (jet) scenarios where high Lorentz factor fireballs can escape the inevitable baryon-polluted slow wind that must accompany the initial energy deposition (e.g., Mészáros & Rees 1992a, b). In such cases, the main part of the observed gamma-ray radiation occurs when the bulk kinetic energy of the baryons (carrying essentially the full energy of the initial fireball) is re-randomized and radiated away in the blast wave being pushed ahead of the relativistically expanding baryons, and in the reverse shock that propagates inwards into the baryonic fireball gas as the latter is decelerated by the external medium (Rees & Mészáros 1992; Mészáros & Rees 1993). This is a very generic mechanism, which operates in almost any scenario for the original energy deposition, as long as it makes a relatively clean, high-entropy initial fireball. Moreover, the process depends on the external environment, thereby allowing the possibility that even a standardized type of fireball could create bursts with a variety of complex time profiles.

The initial development of the fireball determines the final properties of the blast waves, and thus of the bursts. In particular the final bulk Lorentz factor, together with the external density, determines the blast wave burst duration, while the dynamics of the fireball as a function of the baryon loading determines the relative amount of energy in bulk kinetic form (which gets radiated in the blast wave and reverse shock) and in pair and radiation form (which escapes when the fireball thins, usually before the blast wave burst). Since the relativistic dynamics of the fireball expansion determines the entire energetics as well as the temporal characteristics of the burst, a detailed calculation is important.

In this paper we discuss the dynamics of the relativistic fireball expansion from the acceleration stage through the coasting phase, calculating both numerically and analytically the thermodynamic and radiation variables of the flow through the transition to optical thinness and the saturation of the bulk velocity. We discuss the kinematics both in the comoving and laboratory frames, and indicate the scaling of the behavior

[1] Pennsylvania State University, 525 Davey Lab, University Park, PA 16803.
[2] Institute of Astronomy, Madingley Road, Cambridge CB3 0HA, England.

with the various parameters of the problem, extending the treatment to the anisotropic (jet) case. We also consider the role of magnetic fields in the dynamics of the evolution, including the case of magnetically dominated fireballs, and investigate the effect of the magnetic field on the radiative efficiency of the reverse shock that arises when the coasting fireball is decelerated in an external medium.

2. NUMERICAL TREATMENT OF A HIGHLY RELATIVISTIC EXPANDING GAS

2.1. *Computational Approach*

Because of the presence of a natural length in the problem (the initial value of the radius r_0) the gasdynamic equations do not allow an exact similarity solution valid at all radii. For this reason, a numerical solution is the only way to follow exactly the development of the gas, although approximate analytic solutions are possible in the initial acceleration stage and in the later coasting phase (see § 3). Previous calculations of the free expansion of a relativistic gas in spherical symmetry (e.g., Vitello & Salvati 1976, using a characteristics method) have followed the evolution over one and a half decades in the expansion factor. However, expansion over such a limited range is usually not sufficient for the bulk velocity to reach its ultimate saturation value, for the cases of large values of the initial radiation to rest mass energy ratio η considered in many problems, such as the GRB fireball problem,

$$\eta = \frac{E_o}{M_o c^2} \simeq 10^3 E_{51} \left(\frac{M_o}{0.6 \times 10^{-6}\, M_\odot} \right)^{-1} . \qquad (2.1)$$

Here M_o is the total mass of polluting baryons that get mixed in with the photon-pair fireball of energy $E_o \sim 10^{51} E_{51}$ ergs. The latter is of the order of magnitude of the *initial* photon energy expected from the liberation of an amount of gravitational energy $GM_*^2/R_N \sim \epsilon M_\odot c^2 \sim 10^{54}$ ergs, where $\epsilon \lesssim 1$, $R_N \sim 10^6$ cm, most of which goes into neutrinos and gravitational waves.

The numerical treatment of the free expansion of a highly relativistic gas with spherical symmetry calls for the use of Lagrangian hydrodynamics because of the vast range of physical scales present in the problem, of the order of 10 or more decades. We have developed a Lagrangian code for relativistic fluid flows that uses a second-order Runge-Kutta integrator (Benz 1984) with adaptive time step. This method has the advantage that a Courant (Courant, Friedrichs, & Lewy 1928) condition does not limit the size of the time steps, an essential ingredient in achieving short and long time scales. Relativistic artificial viscous stress was implemented in the code and calibrated using relativistic shock tube problems. This was used to verify the accuracy of the same code when artificial viscosity was switched off, which turns out to be quite good (and significantly faster) in the cases of free expansion treated here. The reason why this is an excellent approximation is that shocks do not normally occur in such free expansion problems. All the runs described below are therefore for zero artificial viscosity. Typically, simulations consisted of 200 Lagrangian grid points (mass shells). Runs with different number of mass shells were done to check the convergence of our results. We monitored the ability of the code to reproduce the analytic solutions of the plane symmetric rarefaction wave traveling inwards (Vitello & Salvati 1976). We found that for 200 grid points the maximum absolute error ($\leq 3\%$) as well as the maximum cumulative error ($\leq 2\%$) appeared in the velocity. In our experiments this Lagrangian scheme was found to be able to handle successfully values of η at least up to 10^{10}, leading to typical final bulk Lorentz factors up to 10^5.

2.2. *Numerical Results*

The initial gas configurations discussed here assume, for simplicity, that the gas at $t = 0$ is uniformly distributed within $r \leq r_o$, having a total rest mass M_o, and that at $t = 0$ an amount of radiation energy $E_o \gg M_o c^2$ is deposited uniformly throughout the spherical gas. This approximation is not very restrictive, since the free expansion behaves essentially ballistically, after a few expansion time scales. The gas is optically thick to its own electrons, and the resulting photon-pair-electron-baryon fluid is essentially an isentropic fluid which can be modeled as a gas of adiabatic index $\gamma_a = 4/3$, as long as the photons are coupled to the matter by radiation drag. The same applies to the case where the energy is mainly in the form of magnetic fields (see § 4). After decoupling, the adiabatic index becomes $\gamma_a = 5/3$. We have carried out calculations for values of η ranging from close to unity up to the pure pair-scattering regime $\eta \sim \eta_p \sim 10^{10}$ (see § 3.3). As a specific example, we discuss the case of $\eta = 10^4$ below, which is characteristic of the relativistic behavior.

In the course of the expansion most of the mass, as seen by a laboratory observer, is concentrated in a thin shell near the leading edge of the expanding gas (cf. also Vitello & Salvati 1976). This is seen in Figure 1, where the distribution of the lab density is plotted as a function of the (normalized) lab radius for $\eta = 10^4$. The curves are plotted at the times (from top to bottom) when the lab frame expansion factor $r(\rho_{mx})/r_o$ (which is proportional to the lab frame time) is equal to 0.2, 0.4, 0.6, 0.8, 1.0 times η.

As the gas expands, the mass shells acquire a bulk velocity which initially increases in time and eventually saturates. The distribution of this bulk Lorentz factor over the various mass shells is shown in Figure 2, for a fireball of $\eta = 10^4$ at the lab times (increasing from botton to top) when $r(\rho_{\max})/r_o = \eta^{1/2}, \eta, \eta^{3/2}, \eta^2, \eta^{5/2}, \eta^3$. One sees that the leading edge reaches a value of $\Gamma \sim \eta$, and most of the mass reaches one-third of that value, at the laboratory time for which the expansion factor

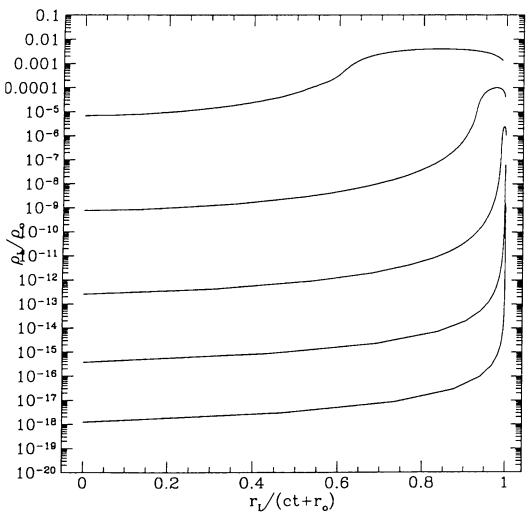

FIG. 1.—Mass distribution in the laboratory frame for a fireball of $\eta = 10^4$ at the times when the lab expansion factor $r(\rho_{\max})/r_o$ (proportional to the lab time) is equal to 0.2, 0.4, 0.6, 0.8, 1.0 times η, from top to bottom.

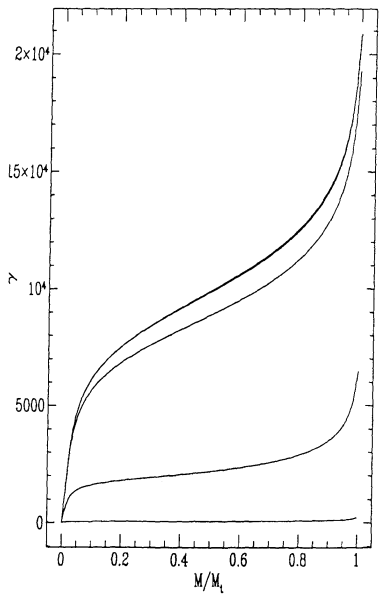

FIG. 2.—Distribution of the bulk Lorentz factor Γ over the various mass shells (i.e., against the Lagrangian mass coordinate), for $\eta = 10^4$, at the times when the lab expansion factor (which is proportional to the lab time) is $r(\rho_{max})/r_o = \eta^{1/2}, \eta, \eta^{3/2}, \eta^2, \eta^{5/2}, \eta^3$, from bottom to top.

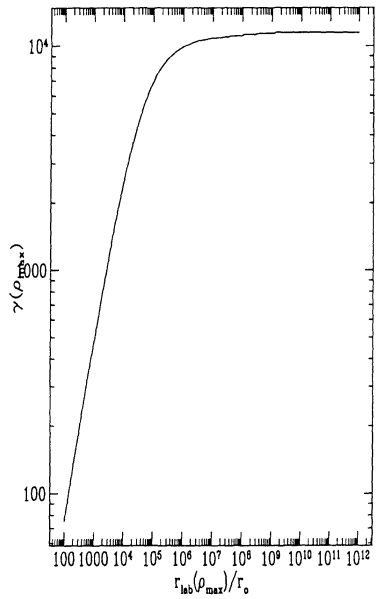

FIG. 3.—Average bulk Lorentz factor Γ as a function of the expansion factor $(\rho_{max})/r_o$, for $\eta = 10^4$.

$r(\rho_{mx})/r_o \sim r_s/r_o \sim \eta$. After that the average bulk Lorentz factor of most of the matter saturates to the value $\Gamma \sim \eta$, while the leading edge remains within a factor 2 of that value, and the trailing edge of the inner 10% of the matter tapers off fairly steeply to zero.

The average bulk Lorentz factor (or what is nearly the same, $\Gamma(\rho_{max})$ where the density is maximal) grows initially linearly with radius, and saturates to a value $\Gamma \sim \eta$ after a (lab) expansion factor equal to η. This is seen in Figure 3, where $\Gamma(\rho_{max})$ is plotted against the expansion factor $r(\rho_{max})/r_o$.

Within the thin shell containing most of the mass, called the mass envelope shell, the bulk of the mass (say, the inner 80% away from the outer and inner edges) is distributed quite uniformly, even after the average bulk Lorentz factor has saturated (for $r(\rho_{max})/r_o \gtrsim r_s/r_o \sim \eta$). Only later, particularly after $r(\rho_{max})/r_o \gtrsim r_b/r_o \sim \eta^2$, a slight asymmetry favoring the leading edge of the envelope shell starts to become apparent, but even then the matter within the shell can be considered uniform to a good approximation. This is shown in Figure 4*a*, where the lab frame density ρ_L is plotted against the Lagrangian mass coordinate M/M_t (where $M_t \equiv M_o$ is the total rest mass, which is

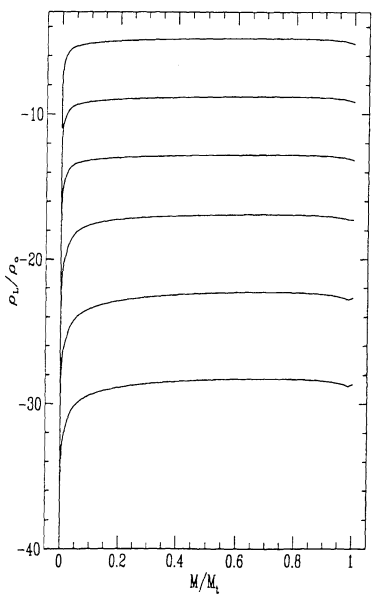

FIG. 4*a*

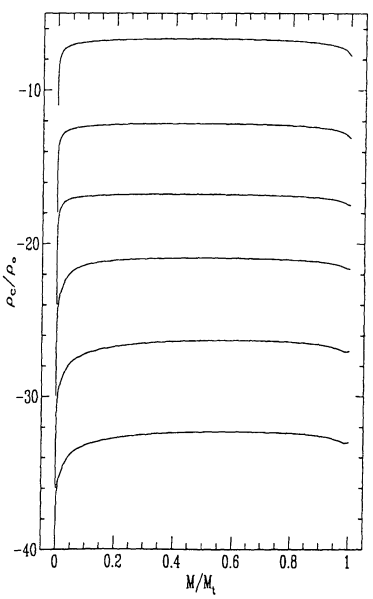

FIG. 4*b*

FIG. 4.—(*a*) Lab frame mass density against the Lagrangian mass coordinate, at the times (from top to bottom) when the expansion factor is $r(\rho_{max})/r_o = \eta^{1/2}, \eta, \eta^{3/2}, \eta^2, \eta^{5/2}, \eta^3$. (*b*) Comoving frame mass density against the Lagrangian mass coordinate, for the same instants as (*a*).

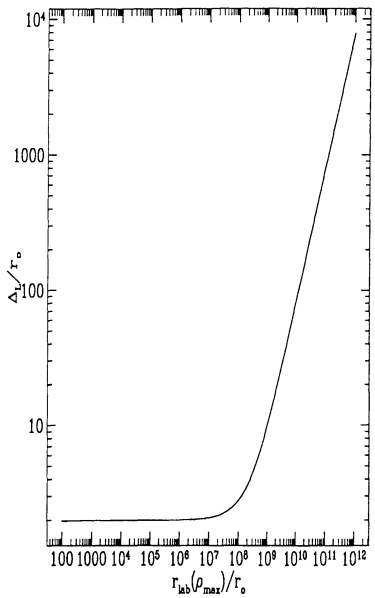

FIG. 5a

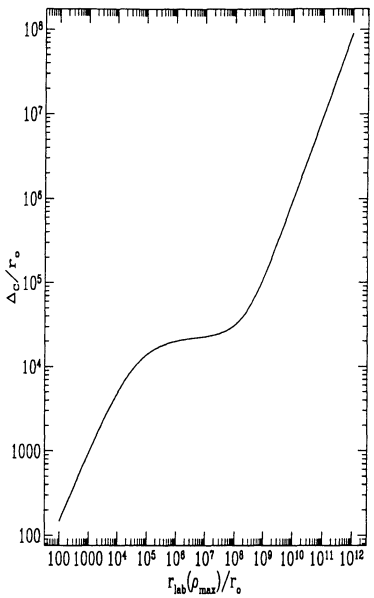

FIG. 5b

FIG. 5.—(*a*) Lab frame width of the shell where most (80%) of the mass is located, as a function of the expansion factor $r(\rho_{max})/r_o$, for $\eta = 10^4$. (*b*) Comoving frame width of the shell containing most (80%) of the matter, as a function of the expansion factor $r(\rho_{max})r_o$, for $\eta = 10^4$.

mostly within the shell). In Figure 4*b* we show the same plot for the comoving mass density ρ_c. The latter is even more uniform than the laboratory frame density. Thus, a comoving observer would find that the world around it is essentially isotropic and homogeneous, at least far from the edges, but with a density that drops in time, as seen from the decreasing value of the average density. The various curves, from top to bottom, are for increasing times when the expansion factor $r(\rho_{mx})/r_o$ is equal to $\eta^{1/2}, \eta, \eta^{3/2}, \eta^2, \eta^{5/2}, \eta^3$.

The width of the mass envelope shell in the lab frame is initially nearly constant an equal to the initial radius, $\Delta r/r_o \sim 1$ (see also Vitello & Salvati 1976; Goodman 1986). This remains so, however, only until an expansion factor $r(\rho_{max})/r_o \sim r_b/r_o \sim \eta^2$ is reached. After that, the lab width starts to grow linearly (see Fig. 5*a*). The comoving frame width, for its part, grows initially linearly with the expansion factor until η, remains approximately constant between η and η^2, and then resumes a linear growth with radius (Fig. 5*b*). The physical reason for this behavior is discussed in § 3.

We have also calculated numerically the lab radius at which an expanding fireball becomes Thomson optically thin against its own electrons, as a function of the initial radiation energy to rest mass ratio η. This condition is computed in the comoving frame, being the same in the lab frame, as it should, since the optical depth of a constant amount of mass is an invariant between reference frames. This (lab) thinning radius r_t is found to vary as $\eta^{-1/2}$, in excellent agreement with the analytic estimate (3.13). Another quantity of interest is the value of the average bulk Lorentz factor Γ_t at which fireballs of varying η become optically thin, as a function of η. The numerically computed value of Γ_t grows linearly with η for low values of η at which optical thinness is achieved before the bulk velocity Γ saturates to η, and Γ_t decreases as $\eta^{-1/2}$ for larger values of η at which thinness is achieved after the bulk Lorentz factor has saturated (in agreement with Shemi & Piran 1990). The linear decrease $\propto \eta^{-1/2}$ changes to η^0 for very large values of η (or initial radiation energies sufficiently larger than $M_o c^2$) at which the opacity of the fireball at optical thinness is still dominated by the pairs (instead of by the polluting baryonic electrons). This occurs for $\eta \gtrsim 0.6 \times 10^{10}$, above which $r_t \sim$ constant, $\Gamma_t \sim 2.4 \times 10^3 \sim$ constant (see § 3).

3. ANALYTICAL TREATMENT OF THE FIREBALL DYNAMICS

3.1. *Accelerated and Saturated Expansion*

A fireball expanding into a low-density external environment may, in its initial stages, be considered to be expanding in a vacuum. Thus, as long as the inertia of the accumulated external matter can be neglected, shocks will not play an important role in the energetics. Pressure gradients may exist in the expanding fireball gas, particularly if the initial density and pressure distribution is inhomogeneous, but free (unimpeded) expansion will tend to stretch these out. One may therefore, as a first approximation, neglect internal pressure gradients. Thus, even though we are dealing with a fluid, the dynamics of the expansion would be expected initially to resemble that of a collisionless gas of relativistic particles. The particles initially have an isotropic velocity distribution within a radius r_o, with an initial random Lorentz factor $\gamma = \eta = E_o/M_o c^2$. But as they expand, the velocity distribution viewed in the lab frame will become increasingly anisotropic. For the ballistic expansion in the lab frame, when the particles have reached a radius r their velocity vectors will be confined within an angle $(r/r_o)^{-1}$ of the radial direction. A transformation to a frame of reference which is outwardly moving with a bulk Lorentz factor

$$\Gamma \sim (r/r_o) \tag{3.1}$$

makes the particle velocity distribution appear again isotropic. This frame is, therefore, the comoving frame of the expanding particles in the initial acceleration phase, which moves outward with a velocity increasing according to $\Gamma \propto r$. [For a

jet geometry of opening angle θ there is an approximate angular scaling in equation (3.1) so that $\Gamma \sim \theta(r/r_0)$; see below.]

The expansion occurs at the expense of the comoving frame thermal energy E, which must therefore drop as $E \propto r^{-1}$. This follows from the adiabatic behavior for a relativistic gas

$$E/E_o = T/T_o = (\rho/\rho_o)^{1/3} = (V_o/V)^{1/3} , \tag{3.2}$$

where E, T, ρ, V are comoving energy, temperature, density, and volume, provided $V \propto r^3$ in the initial (linear expansion) stage, where r is lab radius. The latter can be seen from the fact that the laboratory frame radial extent of the particles in free expansion is expected to be (initially, at least) $\Delta r \sim r_o$, while the comoving radial width ΔR is related to the corresponding lab width through $\Delta R = \Delta r\Gamma$ (we denote comoving radii with capital R and laboratory radii with lower case r). Since the dimensions transverse to the motion will be the same in the lab and comoving frame, the comoving volume in this (acceleration) phase is $V \propto r^2\Delta R \propto r^2 r_o \Gamma \propto r^3$.

The accelerating behavior $\Gamma \propto (r/r_o)$, however, can only go on as long as the internal energy of the expanding gas is relativistic. After the comoving energy density drops below the baryon rest mass density ρc^2, the bulk Lorentz factor Γ must saturate to the maximum value it can acquire, which is approximately the initial thermal Lorentz factor η in the case of significant baryon loading, or more generally

$$\Gamma_s \sim \min [\eta, \Gamma_m] , \tag{3.3}$$

where the second value is appropriate for $\eta > \Gamma_m$ given in equation (3.14), as shown in § 3.4.

The initial acceleration and the saturation behavior can also be obtained from a phenomenological expression for the average bulk Lorentz factor (e.g., Shemi & Piran 1990, Piran, Narayan, & Shemi 1992)

$$\Gamma \sim \frac{E_o + M_o c^2}{E + M_o c^2} = \frac{\eta + 1}{\eta(E/E_o) + 1} = \frac{\eta + 1}{\eta(V_o/V)^{1/3} + 1} , \tag{3.4}$$

making the analogy with a section of the expanding universe, that is, assuming spherical symmetry, homogeneity, and isotropy. Here E is the fluid thermal energy density (initially mainly in photons and leptons, with an admixture of M_o baryons). As long as it is optically thick and $\eta \gtrsim 1$, the pressure is radiation-dominated throughout the expansion, and the adiabatic exponent is 4/3, as implied in equation (3.2). In the linear expansion phase, we can take (from the discussion below equation [3.1]) $V^{1/3} \propto r^{-1}$, where r is lab radius, so from equations (3.3) and (3.4) one gets for $E_o/E \ll \eta$ the accelerating behavior $\Gamma \sim E_o/E \sim r/r_o$, while for $E_o/E \gg \eta$ one gets the saturated $\Gamma \to \eta$; (see equation [3.2]). The saturation occurs (in spherical symmetry) at $r_s/r_o \sim \eta$. However, for $\eta > \Gamma_m$ given by equation (3.14), η must be replaced by Γ_m (see § 3.4).

3.2. *Lab and Comoving Geometry*

As the particles move outward with velocity vectors which are increasingly radial, they form a radially expanding shell whose radius is initially $\Delta r \sim r_o$. The radial velocity spread $(v - c)/c \sim \Gamma^{-2}$, and a noticeable departure from the approximately constant width r_o starts to become appreciable only after $r \gtrsim r_b$ where $\Delta r \sim r\,\Delta v/c \sim r_b \eta^{-2} \gtrsim r_o$, or $r_b/r_o \gtrsim \eta^2$. The laboratory frame width is therefore

$$\Delta r \sim \max (r_o, r/\Gamma^2) \sim \begin{cases} r_o, & \text{for } r \lesssim r_b ; \\ r/\Gamma^2 = r/\Gamma_s^2, & \text{for } r \gtrsim r_b . \end{cases} \tag{3.5}$$

The width in the comoving frame is $\Delta R = \Delta r\Gamma$, which from equations (3.1), (3.3), and (3.5) is

$$\Delta R \sim \begin{cases} r_o\Gamma \sim \theta r & \text{for } r \lesssim r_s ; \\ r_o\Gamma_s & \text{for } r_s \lesssim r \lesssim r_b ; \\ r/\Gamma_s & \text{for } r \gtrsim r_b , \end{cases} \tag{3.6}$$

where the two characteristic radii for saturation and for the start of the shell linear expansion in the lab frame are

$$r_s/r_o \sim \theta^{-1}\Gamma_s, \quad r_b/r_o \sim \Gamma_s^2 , \tag{3.7}$$

and Γ_s is given by equation (3.3). The second part of the first line of equation (3.6) follows from the behavior of Γ (eq. [3.10]), which can be derived from equation (3.3), $\Gamma \sim [(V/V_o)^{1/3}, \Gamma_s]$ for $[r \lesssim r_s, r \gtrsim r_s]$, and from the ratio of comoving volumes $(V/V_o) = 2\pi\theta_o^2 r^2 \Delta R/(4\pi/3)r_o^3 = \theta^2(r/r_o)^2(\Delta R/r_o)$. Here we assumed that V possibly consists of two cones (jets) of opening half-angle θ_o, and we define $\theta = (3/2)^{1/2}\theta_o$, where $\theta \sim 1$ for spherical symmetry. Using the above Γ and equation (3.6), we get the comoving volumes in the three different stages of free expansion as

$$V = (4\pi/3)\theta^2 r^2 \Delta R \sim \begin{cases} (4\pi/3)\theta^3 r^3 & \text{for } r < r_s ; \\ (4\pi/3)\theta^2 \Gamma_s r_o r^2 & \text{for } r_s < r < r_b ; \\ (4\pi/3)\theta^2 \Gamma_s^{-1} r^3 & \text{for } r > r_b ; \end{cases} \tag{3.8}$$

and the comoving radiation energy and temperature vary according to

$$\left(\frac{E}{E_o}\right) = \left(\frac{T}{T_o}\right) = (V_o/V)^{1/3}$$

$$= \begin{cases} \theta^{-1}(r_o/r) & \text{for } r < r_s ; \\ \theta^{-2/3}\Gamma_s^{-1/3}(r_o/r)^{2/3} & \text{for } r_s < r < r_b ; \\ \theta^{-2/3}\Gamma_s^{1/3}(r_o/r) & \text{for } r > r_b . \end{cases} \tag{3.9}$$

This is therefore the complete r dependence of the adiabatic law (3.2). The factor θ can be taken to include both an angle dependence and a dependence on the statistical weight factor g in the equilibrium energy density gaT^4. That is, $\theta^{-1} \equiv (g_o/g)^{1/3}\theta'^{-1}$, where $(g_o/g)^{1/3} = (11/4)^{1/3}$ accounts for the change in the statistical factor for the equilibrium energy density when the pairs annihilate as the temperature drops below $kT \lesssim m_e c^2$, and θ' is the angular factor which accounts for the possibility of expansion along a restricted range of solid angles. If we have radial expansion along two jets of solid angle θ_o, and all of the energy is channeled into this solid angle, $\theta' \sim (3/2)^{1/2}\theta_o$. If the gas uses some of its internal energy to perform work against a medium which prevents escape in the directions outside of the jet angles θ_o, then the effective $\theta' < (3/2)^{1/2}\theta_o$. In the discussion below (and in the numerical calculations of § 2) we have ignored the small shift of the curves associated with the change of the statistical factor, that is, we simplify to $(g_o/g) \sim 1$, $\theta \sim \theta'$. (Note that this angular factor is only approximately correct, since it does not account for any possible lateral expansion or transverse radiation loss of the jet; it is strictly valid for one-dimensional radial variations within the angle θ'.)

The behavior of Γ, from the discussion following equation (3.7) and (3.9) is therefore

$$\Gamma \sim \begin{cases} \theta(r/r_o) & \text{for } r < r_s ; \\ \Gamma_s & \text{for } r_s < r < r_b ; \\ \Gamma_s & \text{for } r > r_b , \end{cases} \tag{3.10}$$

and r_s, r_b are given by equations (3.7) and (3.3). Thus, for a jet, the asymptotic accelerated behavior has a similar radial dependence as the spherical case, but the same bulk Lorentz factor is achieved at radii which are higher by θ^{-1}. This is because at the same radii the jet, being confined to narrower angles, has a larger internal entropy than the spherical flow. Also the saturation radius is larger by θ^{-1} in the jet case. However, both the jet and the spherical flow must saturate to the same final bulk Lorentz factor Γ_s given in equation (3.3), namely either to η or to Γ_m, whichever is smaller (see § 3.2, eq. eq. [3.14]).

3.3. *Optical Depth and Saturation Lorentz Factor*

Depending on the value of $\eta = E_o/M_o c^2$, the scattering depth of the fireball at optical thinness is dominated by the "polluting" baryonic electrons (when $\eta < \eta_p$, where the latter is given by eq. [3.19]), or, if the fireball has very low baryon pollution, the scattering opacity previous to reaching optical thinness is dominated by the $e^{\pm}$ pairs (Goodman 1986; Paczyński 1986; Shemi & Piran 1990), when $\eta > \eta_p$.

1. *Electron-dominated scattering.* In the case $\eta < \eta_p$, when baryonic electrons dominate at thinness, the optical depth is

$$\tau = \frac{M_o/m_p \sigma \Delta r}{4\pi r^2 \theta^2 r^2 \Delta r} = \left(\frac{E_o \kappa}{4\pi r_o^2 c^2}\right) \frac{1}{\theta^2 \eta} \left(\frac{r_o}{r}\right)^2 = \Gamma_m^3 \theta^{-2} \eta^{-1} \left(\frac{r_o}{r}\right)^2 . \tag{3.11}$$

Here σ is the scattering cross section, $\kappa = \sigma/m_p \sim 0.4$ cm^2 g^{-1}, and Γ_m is given in equation (3.14). The initial optical depth is $\tau_o = \Gamma_m^3 \theta^{-2} \eta^{-1} = \Sigma_o \kappa = \eta^{-1} \Sigma_{r,0} \kappa$, where

$$\Sigma_o \equiv M_o/4\pi r_o^2 \theta^2, \quad \Sigma_{r,o} \equiv E_o c^{-2}/4\pi r_o^2 \theta^2 = \Sigma_o \eta \tag{3.12}$$

are the initial baryon mass surface density and the initial radiation equivalent mass surface density. In the course of the expansion, the gas becomes optically thin at a radius r_t defined by

$$\frac{r_t}{r_o} = \Gamma_m^{3/2} \theta^{-1} \eta^{-1/2} = (\Sigma_o \kappa)^{1/2} = \tau_o^{1/2} = 1.9 \times 10^8 E_{51} r_6^{-1} \theta^{-1} \eta^{-1/2} , \tag{3.13a}$$

or

$$r_t = \left(\frac{E_o \kappa}{4\pi \theta^2 c^2 \eta}\right)^{1/2} = 1.9 \times 10^{14} \theta^{-1} E_{51}^{1/2} \eta^{-1/2} \text{ cm} , \tag{3.13b}$$

where the initial energy E_o and radius r_o have been arbitrarily normalized to 10^{51} ergs and 10^6 cm, and the second version (3.13b) is independent of r_o. The critical Lorentz factor Γ_m and the critical η_m are defined as

$$\Gamma_m \equiv \eta_m = (\tau_o \eta)^{1/3} = (\Sigma_o \kappa \eta)^{1/3} = (\Sigma_{r,o} \kappa)^{1/3} = \left(\frac{E_o \kappa}{4\pi r_o^2 c^2}\right)^{1/3} = 3.3 \times 10^5 E_{51}^{1/3} r_6^{-2/3} . \tag{3.14}$$

This is the maximum possible bulk Lorentz factor achievable for a given initial radiation energy E_o deposited within a given initial radius r_o (§ 3.4). It is also, for a given E_o and r_o, the "critical" value of $\eta = \eta_m$ (reached at a critical loading mass $M_o = M_m = [E_o/\eta_m c^2]$) for which the thinning radius (3.13) is equal to the saturation radius $(r_s/r_o) \sim \theta^{-1}\eta$. For a given E_o, as one varies M_o or η, the critical value $\eta = \eta_m = \Gamma_m$ is reached at a radius r_m given by

$$\frac{r_m}{r_o} = \frac{r_s}{r_o} = \frac{r_t}{r_o} \sim \theta^{-1} \Gamma_m . \tag{3.15}$$

For $\eta < \Gamma_m$, optical thinness is reached after saturation, whereas for $\eta > \Gamma_m$ optical thinness is reached before saturation, so the bulk Lorentz factor at thinning $\Gamma_t = \theta(r_t/r_o)$ is equal to

$$\Gamma_t = [\eta, \Gamma_m^{3/2} \eta^{-1/2}] \quad \text{for } [\eta < \Gamma_m, \Gamma_m < \eta < \Gamma_p] , \tag{3.16}$$

where Γ_p is given by equation (3.20).

2. *Pair-dominated scattering.* For very large η, such that $\eta > \eta_p > \Gamma_m$, the $e^{\pm}$ scattering dominates, instead of baryonic electron scattering, and optical thinness occurs when the pairs fall out of equilibrium, which occurs at a lab radius r_p given by

$$\frac{r_p}{r_o} = \theta^{-1} \frac{T_o}{T_p} \sim 2.4 \times 10^3 E_{51}^{1/4} r_6^{-3/4} \theta^{-1} , \tag{3.17}$$

where $T_p \sim 15$ keV is the temperature where the thermal pair density becomes negligible, and $T_o \sim 36.4 E_{51}^{1/4} r_6^{-3/4}$ MeV is the initial temperature. This occurs during the acceleration stage, so at this point, where pairs become optically thin, Γ has reached the value

$$\Gamma_t = \Gamma_p = E_o/E_p = T_o/T_p = \theta(r_p/r_o) \sim 2.4 \times 10^3 E_{51}^{1/4} r_6^{-3/4} , \tag{3.18}$$

valid for $\eta > \eta_p$. The latter is the value of η above which the pair-dominated regime occurs,

$$\eta_p = \Gamma_m^3/\Gamma_p^2 \sim 0.63 \times 10^{10} E_{51}^{1/2} r_6^{-1/2} \theta^{-1} , \tag{3.19}$$

in terms of which one can write the Lorentz factor and the radius at which pairs become optically thin as

$$\Gamma_p = \frac{\Gamma_m^{3/2}}{\eta_p^{1/2}} , \quad \frac{r_p}{r_o} = \theta^{-1} \Gamma_p = \theta^{-1} \frac{\Gamma_m^{3/2}}{\eta_p^{1/2}} . \tag{3.20}$$

3.4. *Photon Drag and Final Baryon Lorentz Factor*

Photons are obviously coupled to the baryons when $\tau > 1$, which ensures a radiation-like equation of state with adiabatic index 4/3. However, even after $\tau < 1$, baryons may remain coupled to the photons if the density of the latter is so large that the Compton drag time is shorter than the expansion time in the comoving frame. The comoving Compton drag time is the time during which an electron sweeps up an amount of photons whose mass equivalent equals one proton plus one electron's mass, $t_D \sim m_p c^2/\sigma_T c u_\gamma$, where u_γ is the comoving photon energy density. This is longer than the Compton cooling time by a factor m_p/m_e. The ratio of the comoving baryon rest mass energy density u_m and the comoving photon energy density u_γ is

$$\epsilon \equiv \frac{u_\gamma}{u_m} = \frac{E}{M_o c^2} = \eta \frac{E}{E_o} \begin{cases} \theta^{-1} \eta (r_o/r) & \text{for } r < r_s ; \\ \theta^{-2/3} \eta \Gamma_s^{-1/3} (r_o/r)^{2/3} & \text{for } r_s < r < r_b ; \\ \theta^{-2/3} \eta \Gamma_s^{1/3} (r_o/r) & \text{for } r > r_b . \end{cases} \tag{3.21}$$

Dividing the Compton drag time t_D by the comoving expansion time $t_{ex} \sim \Delta R/c$ and multiplying and dividing by the co-

moving baryon density n (comoving baryon rest energy density u_m), the ratio of the Compton drag time to the comoving expansion time is

$$\xi \equiv \frac{t_D}{t_{ex}} = \frac{u_m}{u_\gamma \tau} = \frac{1}{\epsilon\tau} = \begin{cases} \theta^3 \Gamma_m^{-3} (r/r_o)^3 & \text{for } r < r_s; \\ \theta^{8/3} \Gamma_m^{-3} \Gamma_s^{1/3} (r/r_o)^{8/3} & \text{for } r_s < r < r_b; \\ \theta^{8/3} \Gamma_m^{-3} \Gamma_s^{-1/3} (r/r_o)^3 & \text{for } r > r_b, \end{cases} \tag{3.22}$$

where τ is the optical depth (3.11). The final decoupling of photons and baryons occurs at a radius r_f where $\zeta = 1$, or at the thinning radius r_t, whichever is largest.

The final bulk Lorentz factor of the baryons is the value that it has at decoupling from the photons, either when the fireball becomes optically thin or when the Compton drag has become longer than the expansion time, $\zeta > 1$, whichever occurs last. For $\eta < \Gamma_m$, the fireball saturates to a value $\Gamma = \eta$, and thinning occurs at a radius larger by a factor $(r_t/r_s) = (\Gamma_m/\eta)^{3/2} > 1$ where $\zeta_t = (\Gamma_m/\eta) > 1$, so the final baryon Lorentz factor is $\Gamma_f \equiv \eta$ in this case. On the other hand, for $\eta > \Gamma_m$, at optical thinness $\epsilon_t = (\eta/\Gamma_m)^{3/2} > 1$ and $\zeta_t = (\Gamma_m/\eta)^{3/2} < 1$, so the Compton drag keeps photons and baryons coupled beyond r_t. This means that, even though most photons do not collide, most electrons do keep colliding with a small fraction of the photons, and keep being accelerated (with their baryons). They finally decouple when $\zeta_f = 1$ at $(r_f/r_o) = \theta^{-1}\Gamma_m$, where $\Gamma_f \sim \Gamma_m$, $\epsilon_f = (\eta/\Gamma_m) > 1$, and $\tau_f = (\Gamma_m/\eta) < 1$. The terminal baryon bulk Lorentz factor is therefore

$$\Gamma_f = \min(\eta, \Gamma_m) . \tag{3.23}$$

This is equal to the Lorentz factor at thinning Γ_t in the case $\eta < \Gamma_m$ when $\Gamma_t = \Gamma_f = \eta$, but $\Gamma_t < \Gamma_f$ when $\eta > \Gamma_m$.

3.5. *Baryon Loading and Final Radiation to Kinetic Energy Ratio*

One can distinguish four baryon-loading regimes, characterized by the value of η, whose mass limits depend on E_{51}

(H) High-load fireballs, for $1 < \eta < \Gamma_m$, or $0.6 \times 10^{-3}\ M_\odot \lesssim M_o \lesssim 1.8 \times 10^{-9}\ M_\odot$. In this regime Γ grows linearly with r/r_0 until reaching $r_s/r_o = \theta^{-1}\eta$, where it saturates to η, and becomes optically thin at $r_t/r_o = \Gamma_m(\Gamma_m/\eta)^{1/2} > \Gamma_m > r_s/r_o$. The observer-frame (Doppler blueshifted) energy of the radiation escaping under the assumption of isotropy (even if in reality it is beamed) and the kinetic energy of the baryons is

$$E_{r,ob} = E_o \theta^{-2/3} \eta^{-1/3} \left(\frac{r_o}{r_t}\right)^{2/3} = E_o \left(\frac{\eta}{\Gamma_m}\right) < E_o ,$$

$$E_k = M_o c^2 \eta \simeq E_o . \tag{3.24}$$

That is, the thinning radiation burst is a small fraction of E_o (unless $\eta \to \Gamma_m$), most of the energy having gone into the kinetic energy of the baryons.

(C) Critical-load fireballs, for $\eta = \Gamma_m$ or $M_o \sim 1.8 \times 10^{-9}\ M_\odot$. In this case $\Gamma_s = \Gamma_m$ at $r_s = r_t = r_f$, and both the observer-frame radiation energy and the baryon kinetic energy assume their maximal value, $E_{r,ob} \sim E_o/2$, $E_k \sim E_o/2$.

(L) Low-load or underloaded fireballs, for $\Gamma_m < \eta < \eta_p$, or $1.8 \times 10^{-9}\ M_\odot \lesssim M_o \lesssim 0.95 \times 10^{-13}\ M_\odot$. For these (rather low) values of the pollutant mass, Γ grows linearly with r/r_o until becoming optically thin at $r_t/r_o < r_s/r_o \sim r_m/r_o$, where it has the value $\Gamma_t \sim \theta(r_t/r_o) = \Gamma_m(\Gamma_m/\eta)^{1/2} < \eta$. Most of the radiation energy escapes from here without further scattering, while the baryons continue coupled by Compton drag to a small fraction of the photons until the radius r_f where $\Gamma_f = \Gamma_m$. The bulk of the observer-frame radiation energy observed (assumed over 4π) and the final kinetic energy of the protons are

$$E_{r,ob} \sim E_o \theta^{-1} \left(\frac{r_o}{r_t}\right) \Gamma_t \sim E_o ,$$

$$E_k = M_o c^2 \Gamma_f \sim E_o \left(\frac{\Gamma_m}{\eta}\right) < E_o . \tag{3.25}$$

(P) Pair fireballs, for $\eta > \eta_p$ or $M_o \lesssim 0.95 \times 10^{-13}\ M_\odot$. In this extremely underloaded regime, the pairs dominate the Thomson opacity, and the value of Γ grows linearly with r/r_o but it always becomes optically thin at the same value of the radius where $\Gamma \sim \Gamma_p$, $r_t/r_o = r_p/r_o \sim \theta^{-1}\Gamma_p$, given by equations (3.18)–(3.20), independent of η as long as the latter is greater than η_p. The observer-frame radiation energy at thinness under the assumption of isotropy and the final kinetic energy of the baryons is again given by equation (3.25).

In the cases described above, the "thinning" burst (arising when $\tau \sim 1$) is unlikely to be the main burst observed. The significance of the ratio of observed radiation energy to kinetic energy, in our "standard" model (Mészáros & Rees 1993), is that this represents the ratio of the energy in a short precursor burst to that in the main burst, the latter coming from the recovery of the kinetic energy upon interaction with the external medium (§ 4).

4. MAGNETIC FIELDS, EFFICIENCY, AND PHOTON ENERGIES

4.1. *Magnetic Fireballs*

In almost any model of the initial energy release, the initial mass motions are expected to be extremely violent ($v \sim c$), and this could magnify any pre-existing magnetic fields, via compression, shearing, turbulent dynamo mechanisms, Parker-type instabilities, etc. (e.g., Usov 1992; Narayan, Paczyński, & Piran 1992; Thompson & Duncan 1993). If the initial total "disposable" energy (i.e., that portion of the available gravitational energy that is not lost in the form of neutrinos) is $E_o = 10^{51} E_{51}$ ergs, this might be distributed between radiation and magnetic components as

$$E_{B_o} = \xi E_o, \quad E_{ro} = (1 - \xi) E_o , \tag{4.1}$$

where $\xi \leq 1$. One may define separate magnetic and radiation η parameters

$$\eta_B = E_{B_o}/M_o c^2 = \xi\eta, \quad \eta_r = E_{ro}/M_o c^2 = (1 - \xi)\eta \tag{4.2}$$

in terms of the usual total $\eta = E_o/M_o c^2$, with $\eta = \eta_B + \eta_r = \xi\eta + (1 - \xi)\eta$. Even if the magnetic fields have a large-scale structure, the expansion is essentially isotropic in the comoving frame, and therefore the magnetic energy density will evolve $\propto V^{-4/3}$, so the total magnetic energy and radiation energy in the comoving frame vary in a similar manner, $E_B/E_{B_o} = B^2/B_o^2 = E_r/E_{r_o} = (V/V_o)^{-1/3}$, where the volume factors are given by equations (3.9). The bulk Lorentz factor, similarly to equation (3.4), is again

$$\Gamma = \frac{E_o + M_o}{E_r + E_B + M_o} = \frac{\eta + 1}{\eta_r(E_r/E_{ro}) + \eta_B(E_B/E_{B_o}) + 1} = \frac{\eta + 1}{\theta^{-1}(r_o/r)\eta + 1} , \tag{4.3}$$

so that, as in the case of pure radiation, $\Gamma \sim \theta(r/r_o)$ for $r \lesssim r_s$ while $\Gamma \sim \Gamma_s$ for $r \gtrsim r_s$, with $r_s/r_o = \theta^{-1}\Gamma_s$ and $\Gamma_s = \min(\eta, \Gamma_m)$, where Γ_m is given by equations (3.14). The behavior is therefore the same as in § 3, even if all the disposable energy E_o goes into magnetic fields ($\xi \to 1$), that is, for a purely magnetic fireball. The maximal initial magnetic field will be

$$B_o = (8\pi\xi E_o/V_o)^{1/2} \sim 10^{17}\xi^{1/2}E_{51}^{1/2}r_6^{-3/2}\ \mathrm{G}\ , \qquad (4.4)$$

and the comoving field strength evolves according to

$$\left(\frac{B}{B_o}\right) = \begin{cases} \theta^{-2}(r_o/r)^2 & \text{for } r < r_s; \\ \theta^{-4/3}\Gamma_s^{-2/3}(r_o/r)^{4/3} & \text{for } r_s < r < r_b; \\ \theta^{-4/3}\Gamma_s^{2/3}(r_o/r)^2 & \text{for } r > r_b, \end{cases} \qquad (4.5)$$

where r_s, r_b are given in equation (3.7). Even after most of the pairs annihilate, the exponentially small fraction of frozen-in surviving pairs is enough to provide the currents needed to support large-scale fields, so that the behavior (4.5) is uninterrupted beyond the radius at which annihilation, optical thinness, photon drag decoupling, etc., occur.

We may also consider briefly the most extreme scenario of magnetic field dominance, that where the initial field B_o is in equipartition not with the disposable energy $E_o \sim 10^{51}E_{51}$ ergs (which, as in supernovae, is of order 10^{-3} of the total liberated binding energy from the gravitational collapse of about a solar mass) but rather with the binding energy itself, $E_b \sim GM_*^2/R_N \sim 10^{54}E_{54}$ ergs. This might occur in a rapidly spinning object, where rotational and shearing motions would imvolve a large fraction of the total binding energy. In this case

$$B_o = B_m \sim 3 \times 10^{18}(\xi/10^3)^{1/2}\ \mathrm{G}\ , \qquad (4.6)$$

where formally, in terms of the first of equations (4.1), $\xi \sim 10^3$. Now, however, η_r is no longer defined as $(1 - \xi)\eta$ but rather just as $\eta_r = E_{r_o}/M_o c^2$. The dynamic considerations are similar to those just described, but the dynamics is entirely described by using η_B instead of η everywhere in § 3, and increasing Γ_m in equation (3.14) by a factor 10 (since $E_{51} \sim 10^3$).

4.2. *Standard Shock Deceleration Model*

The magnetic fields are carried on in the comoving frame of the polluting baryons M_o present originally in the fireball, and continue expanding with the latter and the corresponding electrons plus surviving pairs until the fireball matter is decelerated by the external medium (Rees & Mészáros 1992). For a fireball which has saturated its bulk Lorentz factor to a value $\Gamma_s = \min[\eta, \Gamma_m]$ the deceleration occurs when the mass of external matter swept up by the fireball equals $\Gamma_s^{-1}M_o$; the swept-up external matter is shock heated to a comoving average thermal Lorentz factor $\gamma_s \sim \Gamma_s \sim \eta \gg 1$, while a reverse shock starts to propagate into the adiabatically cooled fireball material, eventually reheating it to a marginally relativistic average random Lorentz factor $\gamma_r \sim \Gamma_r \lesssim 2$. If the forward and reverse shocks are able to build up magnetic fields which approach equipartition with the postshock thermal energies of the particles (similarly to what seems to occur in supernova remnant shocks), both the forward and reverse shock regions can radiate away the entire thermalized bulk kinetic energy of the shock, that is, the entire total initial disposable energy E_o of the event. However, because of the dependence of the radiative efficiency on the magnetic field strength, it is worthwhile to consider departures from shock magnetic equipartition. One needs also to consider the effects of possible frozen-in primordial fields in the fireball ejecta such as discussed in the previous subsection. These can be characterized by an initial strength B_o and may have been amplified by shear or turbulent dynamo effects during the cataclysmic event of the initial energy release, parameterized through ξ defined in the first of equations (4.1).

In order to estimate the radiative efficiency at the deceleration shock, we use the parameters of our "standard" shock model, for example, Mészáros & Rees (1993). For typical parameters, the shock deceleration occurs after the fireball ejecta has saturated (and after it has become optically thin, producing a brief and weak precursor burst). The deceleration radius r_d at which the fireball gas starts to feel the inertia of an external medium of uniform density $n_{\rm ext} = n_1\ \mathrm{cm}^{-3}$ is $r_d/r_o = (\eta_{\rm ext}/\eta^2)^{1/3}$, where $\eta_{\rm ext} = (E_o/V_o n_{\rm ext} m_p c^2)$, or $r_d = (3E_o/4\pi n_{\rm ext} m_p c^2\eta^2)^{1/3}$, which is

$$r_d \sim 10^{16}\theta^{-2/3}n_1^{-1/3}E_{51}^{1/3}\eta_3^{-2/3}\ \mathrm{cm}\ . \qquad (4.7)$$

(For maximal magnetic dominance, one would use $E_{51} \sim 10^3$, $\eta \equiv \eta_B$, $\xi \sim 10^3$, but for the purposes of this example we consider the more conservative case of $E_{51} \sim 1$, $\xi \lesssim 1$, $n_1 \sim 1$.) The comoving width of the forward and reverse shocked shells is η times larger than their laboratory width $\Delta r \sim r_d/\eta^2$, or $\Delta R \sim r_d/\eta \sim 10^{13}n_1^{1/3}\theta^{-2/3}E_{51}^{1/3}\eta_3^{-5/3}$ cm. The comoving expansion time is consequently

$$t_{\rm ex} = \Delta R/c \sim 10^3 E_{51}^{1/3}n_1^{-1/3}\theta^{-2/3}\eta_3^{-5/3}\ \mathrm{s}\ , \qquad (4.8)$$

while the laboratory expansion time (which is the observed GRB burst time, if the shock radiates efficiently) is $\Gamma_s \sim \eta$ times shorter, $\Delta t = r_d/\eta^2 c \sim 1\ \eta_3^{-8/3}$ s. The total number of baryons (protons) involved in the fireball is $N_{p,o} = E_o/\eta m_p c^2 \sim 10^{54}E_{51}\eta^{-1}$, and the comoving density in the preshocked fireball gas (for $r_d > r_b$ in eqs. [3.8] with [3.2]) is

$$n = n_d = N_{p,o}\eta/(4\pi/3)\theta^2 r_d^3 \sim 10^6 n_1^{-1}\eta_3^2\ \mathrm{cm}^{-3}\ . \qquad (4.9)$$

If the reverse shock, whose bulk Lorentz factor achieves at most a value $\Gamma_r \lesssim 2$, produces a shock equipartition field, this is $B_{d,e} = (8\pi n m_p c^2\Gamma_r 4)^{1/2} \sim 10^2 n_1^{-1/2}\eta_3$ G, while if the magnetic field is mainly the original frozen-in field, possibly amplified and adiabatically expanded (eq. [4.4] or [4.6]), this is

$$B_d = 4B_o\theta^{-4/3}\eta^{2/3}(r_o/r_d)^2 = 4 \times 10^{-1}E_{51}^{-1/6}r_6^{1/2}n_1^{2/3}\xi^{1/2}\eta_3^2\ \mathrm{G}\ , \qquad (4.10)$$

where in both cases we have included a factor 4 to take into account the shock compression factor. Aside from the different η dependence, we may consider both the shock-equipartition and frozen-in fields to be given by equation (4.10), where the shock-equipartition field case has $\xi_e \sim 250 n_1^{1/6}E_{51}^{1/6}r_6^{3/2}\xi^{-1/2}\eta_3^{-1}$, while the frozen-in field has $\xi \lesssim 1$ (or $\xi \lesssim 10^3$ in the extreme magnetic dominance case).

4.3. *Radiative Efficiency and Photon Energies*

The efficiency of the blast wave moving ahead of the contact discontinuity can only be affected by the field $B \lesssim B_{d,e}$ developed in the shock, as discussed in our previous papers. Here we focus on the radiative efficiency of the reverse-shocked fireball material, which can be affected by the original, possibly amplified, fireball field B_d of equation (4.10). The "fireball" at the stage just before the reverse shock moves into it contains only a small fraction of the cooled original pairs, and the original polluting baryons and electrons. In the reverse shock, with a field of order (4.10), relativistic electrons with a Lorentz factor $\gamma \sim 10^6$ are sufficient to ensure a comoving synchrotron cooling time $t_{\rm sy} \sim 2 \times 10^3\gamma_6^{-1}E_{51}^{1/3}n_1^{4/3}\eta_3^{-4}$ comparable to the

comoving expansion time (4.8), that is, near unit radiative efficiency, producing photons of characteristic energy $\sim 10\gamma_6^2\xi^{1/2}E_{51}^{-1/6}n_1^{-2/3}\eta_3^3$ MeV in the laboratory frame. The maximum photon energies could well be significantly larger than this, if shock acceleration is considered. If the latter is limited by synchrotron losses, the maximum possible γ is $\gamma_{mx} \lesssim 10^7 B^{-1/2}$ and the maximum energy of the synchrotron photons is $\sim 1\eta_3$ GeV in the laboratory frame, independently of the field strength. For $\eta_3 \sim 1$, synchrotron self-absorption would be negligible for observable radiation in the X-ray or gamma-ray band. Note also that there could be no significant cyclotron line features in the X-ray band, unless $\eta_3 \gtrsim 10^3\xi^{-1/6}$, which would imply too short burst time scales.

Synchrotron losses, however, will almost certainly be surpassed in importance by the inverse Compton (IC) losses of the electrons, in the radiation field of the synchrotron photons. The electrons passing through the shock may energetically attain an average Lorentz factor

$$\gamma \sim (m_p/m_e)\Gamma_r \sim 4 \times 10^3\zeta , \quad (4.11)$$

where $\zeta > 1$ if Fermi-type or other shock acceleration mechanisms are present. The ratio of comoving synchrotron cooling to expansion time $t_{sy}/t_{ex} \sim 5 \times 10^8\gamma^{-1}B^{-2}/t_{ex} \sim 2.5 \times 10^3\zeta^{-1}\xi^{-1}E_{51}^{1/3}n_1^{1/3}\eta_3^{-7/3} \gg 1$ if $\zeta \lesssim 1$, that is, without shock acceleration the synchrotron efficiency would be low. The ratio of the synchrotron photon energy density and the magnetic energy density is $u_{sy}/u_B \sim nP_{sy}\Delta Rc^{-1}/u_B \sim 10^2E_{51}^{1/3}n_1^{-2/3}\theta^{-2/3}\zeta^2\eta_3^{1/3}$, where $u_B = B^2/8\pi$. The ratio of the comoving inverse Compton cooling time to the expansion time is therefore

$$\frac{t_{IC}}{t_{ex}} = \frac{u_B}{u_{sy}}\frac{t_{sy}}{t_{ex}} \sim 2.5 \times 10^1 n_1^2\theta^{2/3}\xi^{-1}\zeta^{-3}\eta_3^{-8/3} , \quad (4.12)$$

giving a first-order inverse Compton efficiency of 4% even for modest average Lorentz factors $\gamma \sim 4 \times 10^3\zeta$ with $\zeta \sim \xi \sim 1$. The synchrotron photons (optical in the comoving frame, X-ray in the lab frame for this γ and $\eta_3 \sim 1$) would be boosted by the single inverse Compton scattering to MeV and GeV energies in the comoving and lab frames.

The radiative efficiency will be larger in the presence of diffusive or other shock acceleration mechanisms producing an electron power-law distribution. If the maximum electron energy achievable is limited by first-order inverse Compton losses, using the Thomson limit in the electron rest frame and balancing t_{IC} with the acceleration time $t_a \sim \gamma/\omega_B$ where $\omega_B = eB/m_e c$, one gets a maximum γ significantly higher than equation (4.11) by a factor $\zeta_m \sim 4 \times 10^1 E_{51}^{1/12}n_1^{7/12}\xi^{1/8}\eta_3^{-7/12}$. However, the synchrotron photon energy in the electron rest frame becomes comparable to the electron rest mass at a slightly lower Lorentz factor, $\zeta_K \sim 10\xi^{-1/6}\eta_3^{-2/3}$. This may be the more appropriate maximum ζ to use for estimating the spectrum, since the Klein-Nishina dropoff in the rest-frame scattering cross section strongly limits the number of photons scattering off electrons more energetic than that. For this value of ζ_K, the synchrotron and first-order IC photons have a characteristic maximum energy of

$$E_{sy} \sim 20E_{51}^{-1/6}n_1^{-2/3}\xi^{1/6}\eta_3^{5/3} \text{ keV} ,$$
$$E_{IC} \sim 10^{13}E_{51}^{-1/6}n_1^{-2/3}\xi^{-1/6}\eta_3^{1/3} \text{ eV} , \quad (4.13)$$

in the lab frame, and a radiation efficiency

$$\epsilon_{sy} \sim 4 \times 10^{-3}E_{51}^{-1/3}n_1^{-1/3}\xi^{5/6}\eta_3^{5/3} ,$$
$$\epsilon_{IC} \sim \min [1, 4 \times 10^1 n_1^{-2}\theta^{-2/3}\xi^{1/2}\eta_3^{2/3}] . \quad (4.14)$$

Another effect which could increase the efficiency is the higher order IC scattering (e.g., Rees 1967). The Thomson optical depth of the fireball shell material is

$$\tau_T \sim n\sigma_T f\Delta R \sim 0.6 \times 10^{-5}E_{51}^{1/3}n_1^{-1}\theta^{-2/3}f\eta_3^{1/3} , \quad (4.15)$$

where $f \leq 1$ is the fraction of the fireball ejecta material that has been heated by the reverse shock. When τ_T is larger than γ^{-2} (as long as the scattering is not Klein-Nishina dominated) the conditions are fulfilled for both first-order and higher order inverse Compton scattering to dominate over synchrotron losses. This is because the synchrotron, first-order IC, second-order IC, etc., photon energy densities are

$$u_{sy} \sim nP_{sy} f\Delta R/c \sim n\sigma_T\gamma^2 u_B f\Delta R \sim \tau_T\gamma^2 u_B , \quad (4.16a)$$
$$u_{IC} \sim nP_{IC} f\Delta R/c \sim n\sigma_T\gamma^2 u_{sy} f\Delta R \sim \tau_T^2\gamma^4 u_B , \quad (4.16b)$$
$$u_{IC'} \sim nP_{IC'} f\Delta R/c \sim n\sigma_T\gamma^2 u_{IC} f\Delta R \sim \tau_T^3\gamma^6 u_B , \ldots \quad (4.16c)$$

and for $\tau_T \gtrsim \gamma^{-2}$ the ratio of the successive energy densities in equation (4.16) are larger by increasing factors of $\tau_T\gamma^2 \geq 1$. Even for $\gamma \sim 10^3$ the IC losses exceed synchrotron losses by a factor 10, and the second-order IC losses would exceed first-order IC losses by another factor of 10, were it not for the fact that for second-order IC and the *maximal* γ the photons in the electron rest frame are now subject to the Klein-Nishina decrease in the cross section. (For $\gamma \sim 10^5$ the respective factors are 10^5, 10^{10}, etc., and the importance of the IC losses makes itself felt already when the shock has heated a small fraction $f \gtrsim 10^{-5}$ of the fireball material.) Notice that for both our simplest model (using the average Lorentz factor $\gamma \sim 10^3$) and for the nonthermal acceleration model with $\gamma_m \sim 10^5$, the first-order IC is in the Thomson limit and exceeds synchrotron losses, but the Klein-Nishina losses diminish the importance (at least as far as the efficiency is concerned) of the second- and higher order IC scattering, although they will affect the spectrum. In the power-law spectrum model, the first-order IC efficiency is unity for $\xi \gtrsim 6 \times 10^{-4}\eta_3^{-4/3}n_1^4\theta^{4/3}$, that is, for initial fields $B_o \gtrsim 2.5 \times 10^{15}n_1^2E_{51}^{1/2}\theta^{2/3}r_6^{-3/2}\eta_3^{-2/3}$ G in the fireball, or for fields developed by turbulent instabilities in the reverse shock which are a factor $10^{-5}n_1^{23/6}E_{51}^{1/6}r_6^{-3/2}\eta_3^{-1/3}$ below equipartition with the mean energy of the reverse post-shock particles, a fairly undemanding assumption. Since the contact discontinuity is likely to be unstable, turbulent mixing of the reverse-shocked fireball gas with the material ahead of the discontinuity could also lead to high radiative efficiencies in the gas behind the forward blast wave.

5. DISCUSSION

We have presented both analytical and numerical calculations of the evolution of a freely expanding ultrarelativistic gas produced by an impulsive energy release. The expansion and cooling from an initially optically thick and extremely hot fireball is followed through the stage where the rest-frame energy density becomes comparable to the rest mass density, where the expansion bulk Lorentz factor, which until then grew proportionally to the expansion factor, saturates to a value which is equal to the smallest of the ratio of the initial thermal energy to rest mass energy in the fireball or the bulk Lorentz factor at which Compton drag becomes negligible. The laboratory and comoving frame geometry as well as the radiation and gasdynamic variables were investigated for a large range of values of $\eta = E_o/M_o c^2$ between 1 and 10^{10}, and we derived analytic scaling laws showing the dependence of the

variables as a function of the various initial parameters, including an approximate angular scaling for the case of jetlike expansion within a limited range of solid angles.

We have also devoted particular attention to the likely magnetic field content of fireballs. An initial magnetic field, possibly amplified by the violent mass motions in the initial impulsive event, may contribute a dynamically significant fraction of the total fireball energy; there is also the possibility that a field develops in the shock-heated fireball after the ram pressure of an external medium decelerates the expansion. When the fireball runs into an external medium and is decelerated, the efficiency with which the re-randomized energy is radiated depends on the magnetic field strength, and on how the electrons are accelerated by the resultant shocks. (The radiation processes during the deceleration phase which give rise to the typical burst profiles are, fortunately, rather less sensitive to precisely how the fireball was originally formed—the formation mechanism may have resembled the impulsive model discussed in §§ 2 and 3, or alternatively could have been spread over as long as a second, as in the scenarios of Eichler et al. 1989, Usov 1992, Narayan et al. 1992 or Woosley 1993. We find, for a range of assumptions, that inverse synchro-Compton cooling should be extremely efficient in radiating away the kinetic energy of the cooled fireball in a time scale short compared to the expansion time, which gives the right order of magnitude duration and total energy for a gamma-ray burst source, and produces a nonthermal spectrum with the bulk of the energy in the MeV to GeV range.

We thank T. Piran, A. Shemi, and R. Narayan for sending us, at the time of submitting this manuscript, their preprint on the fireball hydrodynamics, in substantial agreement with our results in § 2. This research has been partially supported through NASA NAGW-1522.

REFERENCES

Benz, W. 1984, A&A, 139, 378
Cavallo, G., & Rees, M. J. 1978, MNRAS, 183, 359
Courant, R., Friedrichs, K. O., & Lewy, H. 1928, Math. Ann., 100, 32
Eichler, D., Livio, M., Piran, T., & Schramm, D. 1989, Nature, 340, 126
Fishman, G. 1992, in Proc. Saint Louis Compton GRO Symp., in press
Goodman, J. 1986, ApJ, 308, L47
Hartmann, D. 1992, Comm. Astrophys., 16, 231
Imamura, J. N., & Epstein, R. I. 1987, ApJ, 313, 711
Meegan, L. A., Fishman, G. J., Wilson, R. B., Paciesas, W. S., Brock, M. N., Horack, J. M., Pendleton, G. N., & Kouveliotou, C. 1992, Nature, 335, 143
Mészáros, P., & Rees, M. J. 1992a, ApJ, 397, 570
———. 1992b, MNRAS, 257, 29P
———. 1993, ApJ, 405, 278
Narayan, R., Paczyński, B., & Piran, T. 1992, ApJ, 395, L83
Paczyński, B. 1986, ApJ, 308, L43
Paczyński, B. 1990, ApJ, 363, 218
———. 1992, in AIP Conf. Proc. 265, Gamma-Ray Bursts, ed. W. Paciesas & G. Fishman (New York: AIP), 144
Piran, T., Narayan, R., & Shemi, A. 1992, in AIP Conf. Proc. 265, Gamma-Ray Bursts, ed. W. Paciesas & G. Fishman (New York: AIP), 149
Rees, M. J. 1967, MNRAS, 137, 429
Rees, M. J., & Mészáros, P. 1992, MNRAS, 258, 41P
Shemi, A., & Piran, T. 1990, ApJ, 365, L55
Thompson, C., & Duncan, R. C. 1993, ApJ, 408, 194
Usov, V. V. 1992, Nature, 357, 472
Vitello, P., & Salvati, M. 1976, Phys. Fluids, 19, 1523
Woosley, S. 1993, ApJ, 405, 273
Zdziarski, A. A. 1982, in Accreting Neutron Stars, ed. W. Brinkmann & J. Truemper (MPE Rep. 177), (Garching: Max Planck Institut), 246